

A SURVEY FOR NV ABSORPTION AT $Z \approx Z_{GRB}$ IN GRB AFTERGLOW SPECTRA: CLUES TO GAS NEAR THE PROGENITOR STAR

JASON X. PROCHASKA^{1,2}, MIROSLAVA DESSAUGES-ZAVADSKY³, ENRICO RAMIREZ-RUIZ², HSIAO-WEN CHEN⁴
Draft version February 10, 2022

ABSTRACT

We survey N V absorption in the afterglow spectra of long-duration gamma-ray bursts (GRBs) with the intent to study highly ionized gas in the galaxies hosting these events. We identify a high incidence (6/7) of spectra exhibiting N V gas with $z \approx z_{GRB}$ and the majority show large column densities $N(N^{+4}) \gtrsim 10^{14} \text{ cm}^{-2}$. With one exception, the observed line-profiles are kinematically ‘cold’, i.e. they are narrow and have small velocity offset ($\delta v \lesssim 20 \text{ km s}^{-1}$) from absorption lines associated with neutral gas. In addition, the N V absorption has similar velocity as the UV-pumped fine-structure lines indicating these high ions are located within $\approx 1 \text{ kpc}$ of the GRB afterglow. These characteristics are unlike those for N V gas detected in the halo/disk of the Milky Way or along sightlines through high z damped Ly α systems but resemble the narrow absorption line systems associated with quasars and some high z starbursts. We demonstrate that GRB afterglows photoionize nitrogen to N^{+4} at $r \approx 10 \text{ pc}$. This process can produce N V absorption with characteristics resembling the majority of our sample and we argue it is the principal mechanism for N^{+4} along GRB sightlines. Therefore, the observations provide a snapshot of the physical conditions at this distance. In this scenario, the observations imply the progenitor’s stellar wind is confined to $r < 10 \text{ pc}$ which suggests the GRB progenitors occur within dense ($n > 10^3 \text{ cm}^{-3}$) environments, typical of molecular clouds. The observations, therefore, primarily constrain the physical conditions – metallicity, density, velocity fields – of the gas within the (former) molecular cloud region surrounding the GRB.

Subject headings: gamma-rays: bursts – interstellar medium

1. INTRODUCTION

Long-duration gamma-ray bursts (GRBs) are believed to have massive star progenitors arising in active star-forming regions of high z galaxies (e.g. Woosley & Bloom 2006). Roughly half of these events have associated UV/optical afterglows and a subset of these have apparent magnitudes sufficient for high-resolution spectroscopy using 10m-class telescopes (e.g. Fiore et al. 2005; Chen et al. 2005). In principle, the power-law afterglow spectrum has imprinted within it features from gas throughout the interstellar medium (ISM) of the host galaxy. This stands in contrast to studies of quasars whose integrated photon output ionizes their ISM⁵ and surrounding gas out to many tens of kpc. Furthermore, although quasar sightlines frequently penetrate foreground, star-forming galaxies (the so-called damped Ly α systems, QSO-DLA; Wolfe et al. 2005), these are probed according to gas cross-section and quasar sightlines should only rarely intersect the small, dense regions undergoing active star-formation (Zwaan & Prochaska 2006).

In these respects, GRB afterglow spectra allow one to probe a diversity of phases in the ISM of star-forming galaxies: the circumstellar material from the massive star progenitor, the H II region produced by the progenitor and neighboring OB stars, the neutral ISM of the host galaxy, and any diffuse gas within the galactic halo. Unfortunately, even though these phases arise at distinct distances along the sightline, the observed spectrum resolves only the relative velocities of the gas. To focus analysis on a specific phase, one is generally forced to isolate a unique ion and/or material associated with a specific velocity.

GRB afterglow spectra reveal large column densities of H I gas and metals associated with the host galaxy ISM (Savaglio et al. 2003; Vreeswijk et al. 2004; Jakobsson et al. 2006). The analysis of the metal-line transitions have localized this neutral gas within the ambient ISM of the host galaxy. Specifically, the detection of fine-structure lines of Si⁺ and Fe⁺ ions places the gas within $\approx 1 \text{ kpc}$ of the GRB afterglow while the detection of Mg I absorption requires the gas to lie at distances greater than $\approx 100 \text{ pc}$ (Prochaska et al. 2006). These conclusions are supported by direct distance determinations based on analysis of line-variability in fine-structure lines ($\approx 100 \text{ pc}$ and 2 kpc from GRB 020813 and GRB 060418 respectively; Dessauges-Zavadsky et al. 2006; Vreeswijk et al. 2007). The majority of afterglow spectra also show high-ion absorption (e.g. C IV) that is offset by several tens to hundred km s^{-1} from the peak optical depth of the neutral ISM (Chen et al. 2007c). This diffuse, ionized gas is also traced by strong transitions of low-ions (e.g. Si II 1526) but without coincident fine-structure absorption. Therefore, the gas must lie at distances greater than a few kpc from the GRB. These characteristics identify the clouds as partially ionized gas within the halo of the GRB host galaxy (Prochaska et al. 2008).

¹ University of California Observatories - Lick Observatory, University of California, Santa Cruz, CA 95064

² Department of Astronomy and Astrophysics, University of California, Santa Cruz, Santa Cruz, CA 95064

³ Observatoire de Genève, 51 Ch. des Maillettes, 1290 Sauverny, Switzerland

⁴ Dept. of Astronomy & Astrophysics and Kavli Institute for Cosmological Physics, 5640 S. Ellis Ave, Chicago, IL, 60637, U.S.A.

⁵ The obvious exception is the gas identified as broad absorption lines in quasar spectra which is located very close to the quasar.

TABLE 1
GRB-NV SAMPLE

GRB	RA	DEC	Instrument	R	Ref
021004	00:26:54.68	+18:55:41.6	UVES	52,000	1
030323	11:06:09.40	−21:46:13.2	FORS2	2,600	2
050730	14:08:17.14	−03:46:17.8	MIKE	30,000	3
050820	22:29:38.11	+19:33:37.1	HIRES	30,000	4
050922C	19:55:54.48	−08:45:27.5	UVES	30,000	5
060206	13:31:43.42	+35:03:03.6	ISIS	4,000	6
060607	21:58:50.40	−22:29:46.7	UVES	43,000	7

REFERENCES. — 1: Fiore et al. (2005); 2: Vreeswijk et al. (2004); 3: Chen et al. (2005); 4: Prochaska et al. (2007a); 5: Piranomonte et al. (2007); 6: Thoene et al. (2007); 7: Ledoux et al. (2006)

TABLE 2
SURVEY SUMMARY

GRB	z_{GRB}	$\log N_{HI}$ (cm^{-2})	[M/H] ^a	W_{1238}^b (Å)	$\log N(N^{+4})$ (cm^{-2})	$\delta(NV)^c$ (km s^{-1})
GRB021004	2.3291	19.00	0.0	0.307 ± 0.008	14.64 ± 0.04	-10 ± 10
GRB030323	3.3720	21.90	> -0.9	0.325 ± 0.043	> 14.35	20 ± 30
GRB050730	3.9686	22.15	−2.3	0.142 ± 0.021	14.09 ± 0.08	5 ± 5
GRB050820	2.6147	21.00	−0.6	0.045 ± 0.007	13.45 ± 0.05	-90 ± 10
GRB050922C	2.1990	21.60	−2.0	0.197 ± 0.026	> 14.19	-20 ± 5
GRB060206	4.0480	20.85	−0.9	0.093 ± 0.010	13.73 ± 0.15	0 ± 15
GRB060607	3.0748	16.80	0.0	-0.009 ± 0.003	< 12.61	

^aGas metallicity derived from low-ion absorption. See Prochaska et al. (2007b) and Dessauges-Zavadsky et al. (2008) for details.

^bRest-frame equivalent width of the N V 1238 transition.

^cEstimated velocity offset between the rough centroid of the N V line-profile and the peak optical depth of the fine-structure lines.

While studies of the gas in the neutral ISM and galactic halo are valuable for studying the physical conditions in star-forming galaxies, these phases offer only indirect constraints on the nature of the GRB progenitor (Ramirez-Ruiz et al. 2002). Of great interest is to identify gas located within the star-forming region or even gas shed by the progenitor itself. To date, however, no study has presented compelling evidence for gas within ≈ 100 pc of the GRB: neither circumstellar material (Chen et al. 2007c), the molecular cloud that presumably beget the progenitor (Tumlinson et al. 2007), nor material associated with a pre-existing H II region (Whalen et al. 2008). Regarding the latter phase, most of the key diagnostics (e.g. Si IV, Al III, Si III, C IV) are either compromised by blending with the Ly α forest or can be confused with a galactic halo component. Presently, there is only indirect evidence for significant column densities of ionized gas near GRB: a number of GRB sightlines exhibit X-ray absorption with implied metal column densities that significantly exceed the neutral ISM column densities measured from the optical spectra (Galama & Wijers 2001; Watson et al. 2007). This result⁶ hints at a large reservoir of highly ionized gas near the GRB which has not yet been revealed by the rest-frame UV spectra acquired by ground-based facilities.

The challenge to identify and study gas close to the GRB has motivated us to survey GRB afterglow spectra for the presence of N V absorption. Because the N⁺ ion has a large ionization potential (IP=77eV), it is difficult to produce N⁺, especially using stellar radiation fields. In the ISM of local galaxies, N⁺ is generally believed to trace collisionally ionized gas either in equilibrium at a high temperature ($T > 10^5$ K) or out of equilibrium due to a post-shocked gas cooling from $T > 10^6$ K (e.g. Indebetouw & Shull 2004a). In terms of GRB studies, however, the GRB event itself and its bright afterglow emit sufficient numbers of $h\nu \approx 80$ eV photons to produce N⁺ gas near the progenitor. Observationally, the N⁺ ion is notable for exhibiting an alkali doublet at $\lambda\lambda 1238, 1242$ in the rest-frame which lies redward of the H I Ly α transition. In GRB sightlines, therefore, this transition (unlike O VI and S VI doublets) does not blend with H I absorption from the Ly α forest, and GRB afterglow spectra that cover Ly α will often provide an analysis of the N V doublet. Indeed, previous studies have reported the detection of the N V doublet along individual sightlines (Vreeswijk et al. 2004; Chen et al. 2005; Thoene et al. 2007).

In this paper we perform a systematic search and analysis of N⁺ gas for a modest sample of $z > 2$ GRBs. We report on the incidence of its detection, its characteristic column density, and compare the line-profiles with other transitions

⁶ There have also been claims of temporal variation in the X-ray absorption spectrum (e.g. Campana et al. 2007) which would also imply significant metals near the GRB afterglow (Lazzati & Perna 2002), but these variations are more naturally explained by the temporal evolution of the intrinsic X-ray spectrum (Butler & Kocevski 2007).

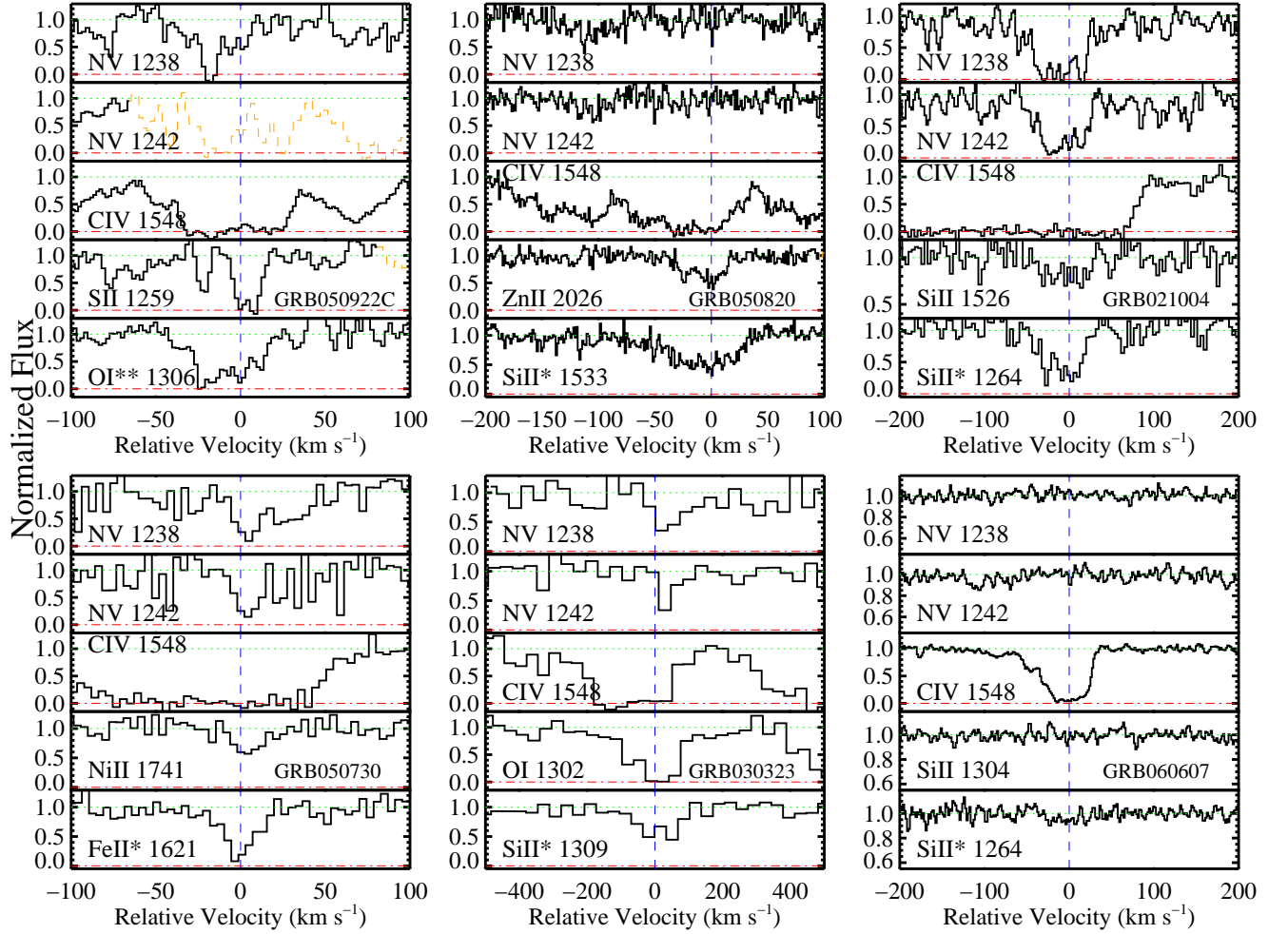


FIG. 1.— Velocity profiles of the N V doublet (top two panels in each sub-figure) compared against a low-ion resonance and fine-structure transition from our sample of GRB afterglow spectra with resolution $R > 2500$. We do not show the data for GRB 060206 (also included in the analysis); the interested reader should see Thoene et al. (2007). With the exception of GRB 060607, the data reveal a positive detection of the N V doublet. Aside from GRB 050820, the N^{+4} line-profiles are relatively narrow and are roughly aligned with the low-ion resonance and fine-structure profiles.

identified along the sightline. Finally, we investigate the origin of this gas and explore constraints on the nature of the GRB progenitor environment.

2. A SURVEY FOR N V ABSORPTION IN GRB SIGHTLINES

2.1. The GRB Sample

Our sample is comprised of all the published and/or publically available GRB afterglow spectra that have resolution $R > 2500$ ($\text{FWHM} < 120 \text{ km s}^{-1}$) and coverage of the Ly α profile and N V doublet from the ISM of the GRB host galaxy. This resolution criterion insures that the N V doublet is well resolved and it also establishes a sensitive detection limit: all of the datasets have a 1σ equivalent width limit of 30 m\AA (or better) corresponding to $N(N^{+4}) = 10^{13.15} \text{ cm}^{-2}$. The sample is summarized in Table 1 and the measured abundances are presented in Table 2. Figure 1 shows the corresponding line-profiles. In every case except GRB 060206, where we adopt the values reported by Thoene et al. (2007), we measured the rest-frame equivalent width of the N V 1238 transition and derived the N^{+4} column density using line-profile fitting techniques and/or the apparent optical depth method (Savage & Sembach 1991). In all but one case (GRB 060607), we report the positive detection of an N V doublet within 100 km s^{-1} of the peak optical depth of the low-ion gas. We associate this gas to the GRB host galaxy.

There are several common characteristics of the sample. First, the peak optical depth and the integrated column densities are large: five of the seven sightlines exhibit saturated N V absorption indicative of a column density $N(N^{+4}) \gtrsim 10^{14} \text{ cm}^{-2}$. Second, these same cases have relatively narrow line-profiles that are aligned or nearly aligned with the peak optical depth of the low-ion profiles. These characteristics are suggestive of a photoionized gas⁷. Third, the N V profiles generally coincide in velocity with the fine-structure lines. By association, we argue the majority of

⁷ Collisional ionization equilibrium would imply $T \gtrsim 10^5 \text{ K}$ and a Doppler parameter for the N gas of $b \gtrsim 15 \text{ km s}^{-1}$. Line-profile analysis of the echelle spectra indicate Doppler widths less than this value (e.g. Dessauges-Zavadsky et al. 2008).

N^{+4} gas is located within ≈ 1 kpc of the GRB event (Prochaska et al. 2006). Finally, there are no significant trends between the characteristics of the N^{+4} gas and the ISM metallicity, GRB redshift, or the H I column density or the metal column density of the ambient ISM.

Two of the seven sightlines do not follow the general trends described above. The first (GRB060607) does not exhibit any N V absorption to very low limits. This sightline is unique for having a very low H I column density and only shows C IV and Si IV absorption at $z \approx z_{GRB}$. The other exceptional system (GRB050820) shows weak, broad N V absorption that is offset by $\delta v \approx -100$ km s $^{-1}$ from the peak optical depth of the low-ions. These characteristics are fundamentally different compared to the remainder of the sample and it suggests that more than one process is responsible for the production of N V gas along GRB sightlines. In the following, however, we will focus on the majority of the sample.

2.2. Comparisons with other N V Surveys

The general characteristics of the GRB N V sample contrast with those for N V samples obtained from quasar sightlines through local and high z galaxies. The most striking difference is the high detection rate of large N^{+4} column densities in GRB sightlines. Fox et al. (2007) have presented the results of a search for N V absorption in sightlines where they also surveyed the O^{+5} ion. They reported only two positive N V detections (each with $N(N^{+4}) \approx 10^{13.5}$ cm $^{-2}$) among six DLAs with both an O VI detection and N V coverage. They set upper limits to the N^{+4} column densities of $< 10^{13}$ cm $^{-2}$ in the remainder of cases. Similarly, an inspection of the public Keck/(HIRES+ESI) DLA database (Prochaska et al. 2007c) indicates the incidence of N V detections to a column density limit of 10^{13} cm $^{-2}$ is less than 20% (see also Fox et al., in prep). Therefore, the GRB sightlines show more frequent and much stronger N V absorption than random sightlines through high z galaxies. Regarding the local universe, the majority of sightlines through the Galactic halo and disk do exhibit N V absorption (Savage et al. 1997), but only a few ($\approx 10\%$) show column densities $N(N^{+4}) > 10^{14}$ cm $^{-2}$ and none have $N(N^{+4}) > 10^{14.5}$ cm $^{-2}$ (Indebetouw & Shull 2004b).

Another important difference is that the N V profiles for GRB are kinematically ‘cold’: they are narrow and have small offset (if any) from the low-ion line-profiles. This contrasts with the majority of Galactic detections whose N V line-profiles are systematically broader than those for low-ions. The Galactic N V lines have Doppler parameters ($b > 30$ km s $^{-1}$; Savage et al. 1997) that generally exceed those observed for the GRB data. By a similar token, very few Galactic N V profiles show peak optical depths $\tau_{1238} > 1$. In short, the profiles characteristic of GRB sightlines, i.e. narrow lines with large peak optical depths, are rarely observed in any astrophysical environment of the local universe. Regarding the N V detections in high z DLA galaxies, the few examples with positive N V detections are comprised of multiple components whose widths more resemble the GRB profiles. These examples, however, have much smaller peak optical depths than the majority of the GRB sample. Furthermore, these lines do not trace the peak optical depths of low-ion gas but are coincident with other high-ions (e.g. C IV, O VI) often with offsets of several tens km s $^{-1}$ from the low-ion features (Fox et al. 2007). The only extragalactic environment where narrow, strong N V profiles have been observed is in gas associated with quasars (e.g. D’Odorico et al. 2004). These associated systems are modeled as photoionized material at distances of a few tens kpc from the QSO. In the following section, we will examine whether a similar process – photoionization by the GRB afterglow – explains our observations.

3. DISCUSSION

The observations presented in the previous section demonstrate the nearly ubiquitous detection of N^{+4} gas at $z \approx z_{GRB}$ in GRB afterglow spectra. The N V absorption lines generally (i) have large peak optical depths with large integrated column densities $N(N^{+4}) \gtrsim 10^{14}$ cm $^{-2}$; (ii) the profiles are relatively narrow (< 50 km s $^{-1}$); (iii) show small velocity offset from fine-structure and resonant low-ion absorption; and (iv) exhibit no significant correlation with other physical characteristics (e.g. metallicity) of the nearby ISM. Similar to the fine-structure lines observed in GRB afterglow spectra (Prochaska et al. 2006), the prevalent detection of strong N V contrasts with sightlines through galaxies in the local and high z universe. Therefore, one infers that processes related to the GRB, its progenitor, and/or its host galaxy must produce the N^{+4} gas. We will now explore possible origins of this gas and its implications for the GRB progenitor environment.

3.1. N V Arising in the Halo and Neutral ISM Gas

We begin by considering the galactic halo⁸ of the GRB host galaxy where one might expect a diffuse, hot baryonic component including N^{+4} gas. This expectation stems from surveys of the Galactic halo where one observes a high covering fraction of high-ion gas including O VI and N V absorption (Sembach et al. 2003; Savage et al. 1997). The relative column densities of these ions, however, do not follow predictions from collisional ionization equilibrium (CIE) models and researchers tend to invoke non-equilibrium scenarios to explain the observations (see Indebetouw & Shull 2004a, for a recent review). These include turbulent mixing layers (Slavin et al. 1993), gas shocked by supernovae remnants (Shull & McKee 1979), and conductive interfaces (Slavin & Cox 1992). None of these models describe all of the Galactic observations and Indebetouw & Shull (2004b) have concluded that several (if not all) of the processes are likely to contribute. It is reasonable to consider whether these processes contribute to the N V absorption observed in GRB afterglow spectra. Several arguments point against this hypothesis. Regarding the theoretical models, none of the mechanisms introduced to explain Galactic N^{+4} gas predict column densities significantly larger than 10^{13} cm $^{-2}$.

⁸ Here, we use the term galactic halo to describe gas that is distinct from the neutral ISM of the galaxy, i.e. we (roughly) associate this component with any gas at scale-heights $\gtrsim 1$ kpc from the plane of the galaxy.

In part, this may be because the models were computed to explain the Galactic data where one rarely finds N^{+4} column densities as large as the GRB sample. Nevertheless, the models cannot reproduce the large N V optical depths unless one presumes a very large number of these layers and/or remnants. This ‘many absorber’ scenario is challenged by the narrow N V profiles observed for the majority of GRB sightlines (Figure 1), especially if one allows that the N abundance in GRB host galaxies is significantly sub-solar (Prochaska et al. 2007b).

Furthermore, several lines of observational evidence challenge interpreting the N^{+4} gas as galactic halo material. First, the GRB N V profiles have large optical depth, are more narrow, and are more tightly correlated with the neutral ISM than the N V profiles observed in the Galactic halo. Second, the coincidence of the N V and fine-structure profiles in velocity space suggests the N^{+4} gas occurs within ≈ 1 kpc of the GRB. This is an indirect argument because N^{+4} does not have its own fine-structure levels. Nevertheless, the coincidence in 4 of 5 sightlines showing N V absorption is statistical evidence that the N^{+4} gas is located near the neutral phase. Note, however, that the difference in ionization potential between these ions means the gas cannot be precisely co-spatial. Third, and perhaps most important, the data support the presence of halo gas but not at the velocities of the N V absorption. Prochaska et al. (2008) have identified low column density features in strong Si II and Fe II transitions that do not exhibit corresponding Si II* or Fe II* absorption. Therefore, these ‘clouds’ lie at distances greater than a few kpc from the GRB afterglow. The clouds tend to show corresponding high-ion absorption (Si IV, C IV) and have relative ionic column densities suggestive of partially ionized gas. Prochaska et al. (2008) associate these clouds with the galactic halo. This halo gas does not exhibit N V absorption and we infer that the clouds which do exhibit N^{+4} gas are unrelated to the halo. Altogether, these theoretical and observational arguments disfavor a galactic halo origin for the majority of N^{+4} gas observed in GRB sightlines. The only obvious exception is the weak, broad N V doublet observed toward GRB 050820 which is also significantly offset from the fine-structure absorption. We await larger GRB samples to assess the frequency of N V detections like this one.

Granted the small velocity offset observed between the N V profiles and the low-ion transitions, one should consider whether the gas is located near the neutral phase, i.e. within the ambient ISM of the galaxy. Indeed, observers have identified N^{+4} gas in the Galactic ISM and even our local bubble (Savage et al. 1997; Welsh & Lallement 2005). Because N^{+4} is not produced by even bright O stars, it must trace interstellar shocks from SN, X-ray emission from hot gas in the ISM, or gas near white dwarfs (e.g. Welsh & Lallement 2005; Dupree & Raymond 1983). In comparison with the GRB observations, however, the observed N^{+4} column densities of the Galactic ISM are generally small ($\lesssim 10^{13} \text{ cm}^{-2}$) and the line-profiles are significantly broader. The values are even extreme for O VI gas in the Galactic ISM (Bowen et al. 2007) which always shows larger column densities than N V gas⁹. One counter-example is observed along the sightline to H1821+643 (Savage et al. 1995). In this case, one observes a strong N V profile that is likely associated with the planetary nebula K1-16. At the redshifts of GRB host galaxies, however, planetary nebulae are rare or non-existent and we expect this process to have a negligible consequence. In summary, although we cannot unambiguously rule out the N V gas arising in the ambient ISM, we consider this to be an unlikely scenario.

3.2. N V Associated with the Starburst Phenomenon

Empirically, one observes N V absorption in the individual and integrated spectra of $z \sim 3$ star-burst galaxies (Lyman break galaxies, LBGs Pettini et al. 2002; Shapley et al. 2003). The VLT/UVES spectrum of the lensed cb58 galaxy (Savaglio et al. 2002), for example, shows a strong N V profile at a velocity consistent with other high-ion and low-ion (resonant and fine-structure) lines observed in the spectrum. All of this gas is offset by $\approx -200 \text{ km s}^{-1}$ from the observed nebular emission lines indicating a galactic-scale outflow, presumably associated with the current burst of star-formation. The physical origin of N^{+4} has not been established for these high z , star-burst galaxies. Nevertheless, if GRB host galaxies are also driving galactic-scale winds (e.g. Thöne et al. 2007; Prochaska et al. 2008), then it is possible that the observed N V absorption is related to this phenomenon. While these mechanisms deserve further attention, we note that the majority of GRB host galaxies are not massive star-bursts but more resemble galaxies like NGC 1705, a local, post star-burst dwarf galaxy (Chen et al. 2007a). While a galaxy like NGC 1705 also may exhibit an outflow (Heckman & Leitherer 1997), the observed P-Cygni N V absorption is not associated with the galactic-scale outflow. In this respect, the N V absorption associated with bright LBGs may not be relevant to the GRB afterglow spectrum.

3.3. Do Stellar Winds Produce N V gas?

Massive stars are observed to generate stellar winds during the course of their main-sequence lifetimes and frequently during the stellar phases that follow. These stars are subject to severe mass-loss throughout their lives, e.g. Galactic stars with initial masses above $\sim 25M_{\odot}$ are thought to lose more than half of their initial mass before their final supernova explosions. Massive stars may pass through several phases having very different stellar winds during their evolution, which may produce a wide variety of structures in the surrounding gas. These stellar winds drive supersonic shock waves into the ambient gas, sweeping and heating it up. Under the presumption that GRB progenitors are massive stars, it is feasible that shocks produced by their stellar wind would produce an observable quantity of N V gas.

The detailed dynamical evolution of the circumburst medium around massive stars is complex. Since massive stars pass through phases with very different mass-loss histories during their evolution, there will be a variety of structures in the surrounding gas. Indeed, at solar metallicities main sequence stars of moderate mass ($25 - 40M_{\odot}$) are thought

⁹ We also note that the O VI lines with largest column densities have the largest Doppler parameters.

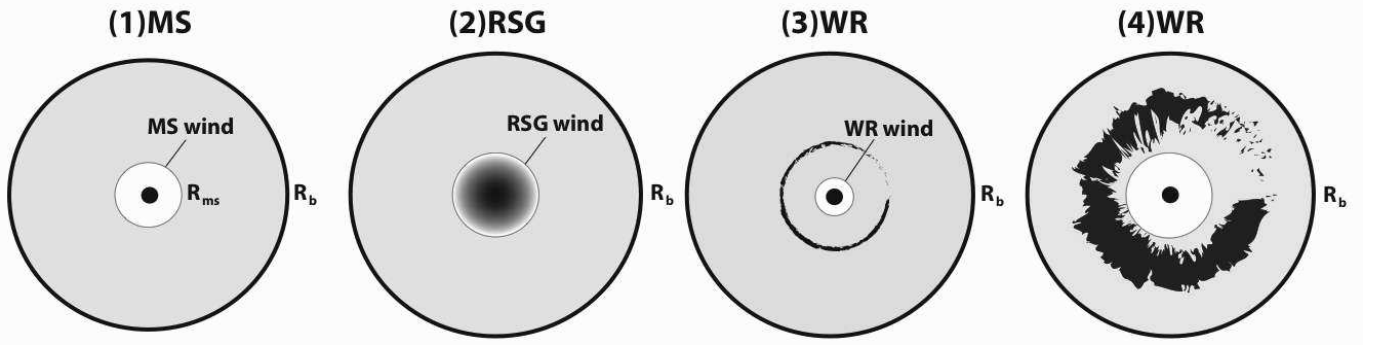


FIG. 2.— A strong wind from a massive star sweeps up the ambient gas forming a stellar wind bubble. Stellar wind bubbles have a double shock structure. An outer shock sweeps up the interstellar medium and forms a thin, radiatively cooled shell of swept-up gas by a contact discontinuity. Since massive stars pass through phases with different mass-loss rates during their evolution, there will be a variety of structures in the surrounding gas (Garcia-Segura et al. 1996). The first, a rarefied, main-sequence wind sweeps up the ambient ISM (1). A dense, slow wind that expands into the rarefied interior of the main-sequence bubble follows as the star evolves through the RSG phase (2). The shell swept up from the main-sequence wind at R_b remains almost constant during this time. This RSG wind forms a dense, high metallicity circumstellar medium surrounding the star. Finally, a fast wind from the WR phase (3) sweeps up this previous slow wind, forming a ring WR nebula. As the WR shell is decelerated by the RSG shell, dense clumps (which have higher inertia) overrun the RSG wind material. After that, the whole interior bubble breaks out and the hot shocked WR wind expands into the remnant main sequence bubble (4).

to develop into red supergiants (RSG) and thereafter Wolf-Rayet (WR) stars. The winds of possible GRB progenitors have been explored by a number of authors (Garcia-Segura et al. 1996; Ramirez-Ruiz et al. 2005; van Marle et al. 2005, 2007; Eldridge et al. 2006). These progenitor stars are thought to be the highly evolved descendants of main-sequence stars with initial masses larger than about $20 M_\odot$.

In these models, there are up to three consecutive types of winds (see Figure 2). The first is a rarefied, fast wind from the main sequence (MS) star that sweeps up the ambient ISM, forming a main-sequence stellar wind bubble. Typical velocities are $v_{\text{ms}} \sim 10^3$ km/s, and mass-loss rates are $\dot{M} \sim 10^{-6} - 10^{-7} M_\odot/\text{yr}$, with lifetimes of $\tau_{\text{ms}} \sim 10^6$ yr (Herrero et al. 1992). A dense and slow wind follows as the star evolves to a RSG phase. This wind expands into the rarefied interior of the main-sequence bubble. This wind forms a dense, high-metallicity circumstellar medium surrounding the star. RSG wind strengths are $v_{\text{rsg}} \sim 10 - 25$ km s $^{-1}$ and $\dot{M} \sim 10^{-4} - 10^{-5} M_\odot \text{ yr}^{-1}$, with lifetimes of $\tau_{\text{rsg}} \sim 10^5$ yr (Humphreys 1991). Finally, a fast wind from the WR phase with $v_{\text{wr}} \sim 10^3$ km/s and $\dot{M} \sim 10^{-5} - 10^{-6} M_\odot \text{ yr}^{-1}$ (Willis 1991), sweeps up the previous slow wind just prior to the death of the star. When the fast WR wind stars blowing, it sweeps up the RSG wind material into a shell, forming the observed WR ring nebula. Finally, the WR ring nebula breaks out of the RSG wind. After that, the hot shocked, WR wind expands into the remnant main sequence bubble.

During the main-sequence phase, the stellar mass-loss increases gradually, while the wind velocity decreases slightly, which results in an almost constant mechanical luminosity

$$L_w = \frac{1}{2} \dot{M}_w v_w^2. \quad (1)$$

This behavior allows us to easily compute the time evolution of the main-sequence bubble using the analytical solutions given by Weaver et al. (1977). Their adiabatic thin-shell solutions are summarized as follows:

$$E_{\text{th}} = \frac{5}{11} L_w t, \quad (2)$$

$$P_b = \frac{7}{(3850\pi)^{2/5}} L_w^{2/5} \rho_0^{3/5} t^{-4/5}, \quad (3)$$

$$R_b = \left(\frac{125}{154\pi} \right)^{1/5} L_w^{1/5} \rho_0^{-1/5} t^{3/5}, \quad (4)$$

where E_{th} is the thermal energy of the hot shocked main-sequence gas, P_b is thermal pressure of the shocked gas, R_b the outer radius and ρ_0 is the ISM constant density. These equations assume that the forward shock is completely radiative, whereas the hot bubble of the shocked wind material is adiabatic, which is a good approximation given that the hot shocked gas radiates poorly. The resulting shocked temperature can thus be estimated by

$$T_{\text{shocked}} = \frac{3}{16} \frac{\mu m_H}{k} \Delta v_w^2 \sim 10^5 \left(\frac{\Delta v_w}{10^2 \text{ km s}^{-1}} \right)^2 \text{ K}. \quad (5)$$

In addition, the above formalism assumes that the ISM is cold, so that it has no significant thermal pressure.

The approximation of a thin shell thus gives an estimate for the size of the circumstellar main-sequence bubble

$$R_b = 52.9 \left(\frac{L_{\text{ms}}}{10^{36} \text{ erg s}^{-1}} \right)^{1/5} \left(\frac{\rho_0}{10^{-23} \text{ g cm}^{-3}} \right)^{-1/5} \left(\frac{t_{\text{ms}}}{5 \times 10^6 \text{ yr}} \right)^{3/5} \text{ pc}. \quad (6)$$

The wind termination shock at the end of the main-sequence phase is located at a radius R_{ms} such that the thermal pressure in the shocked wind material equals the hot bubble pressure. The post-termination shock pressure is roughly equal to the ram pressure in the wind, $P_{\text{ram}} = \rho_{\text{ms}} v_{\text{ms}}^2$, so that

$$R_{\text{ms}} = 7.8 \left(\frac{\dot{M}_{\text{ms}}}{10^{-6} M_{\odot} \text{ yr}^{-1}} \right)^{1/2} \left(\frac{v_{\text{ms}}}{10^3 \text{ km s}^{-1}} \right)^{1/2} \left(\frac{P_{\text{b}}}{3 \times 10^{-12} \text{ dyne cm}^{-2}} \right)^{-1/2} \text{ pc}. \quad (7)$$

Eventually, the star leaves the main sequence and passes through the RSG phase. In the transition phase from main-sequence to RSG stage, the stellar wind increases its density and decreases its velocity. In total, the ram pressure is reduced (i.e. $\rho_{\text{ms}} v_{\text{ms}}^2 \geq \rho_{\text{rsg}} v_{\text{rsg}}^2$), and the wind terminal shock loses its equilibrium position. It collapses and finds a new stationary location on the hydrodynamic timescale of the hot bubble. Once a new equilibrium point is found, a shell of shocked RSG wind stars to build up (although the RSG wind is slow, it is supersonic given its low temperature which results in an extremely low sound speed). After the RSG phase, the star evolves directly to the WR phase. The fast wind sweeps up the previous slow RSG wind material into a shell. L_{wr} exceeds the mechanical luminosity of the RSG wind by several orders of magnitude and as a result, the WR-shell will eventually break out of the RSG wind. After that, the hot shocked, WR wind expands into the remnant main-sequence bubble.

To produce a detectable N V feature, the post-shock temperature must be $T_s \approx 10^5 \text{ K}$ to collisionally ionize nitrogen to N^{+4} and the shock must extend beyond $R \approx 20 \text{ pc}$ to avoid photoionization by the GRB afterglow (see the following section). These constraints rule out an RSG wind as this is too weak to extend beyond a few pc. What is more, the RSG wind is ultimately heated and accelerated to large velocities by the WR wind before core collapse. Meanwhile, the speeds of MS and WR winds lead to a shock temperature $T_s > 10^6 \text{ K}$ (e.g. van Marle et al. 2007). The only exception is in the dense shell of swept-up material at the wind's edge but this rapidly cools to $\approx 10^4 \text{ K}$. Altogether, we conclude that stellar winds associated with the GRB progenitor will not lead to significant N V absorption.

In lieu of shocked gas from a single stellar wind, one could invoke shocks related to an expanding ‘superbubble’, perhaps associated with a starburst (e.g. Tenorio-Tagle et al. 1987). Following equation 5, the appropriate temperature for N V is achieved for an expansion speed of $\approx 100 \text{ km s}^{-1}$. This simple scenario yields the following predictions for a shock-heated N V gas: the N V absorption will be offset by $\delta v \approx -100 \text{ km s}^{-1}$ from the ISM gas and have a Doppler parameter consistent with $T \gtrsim 10^5 \text{ K}$ (i.e. $b \gtrsim 15 \text{ km s}^{-1}$). Reviewing the GRB sightlines comprising our sample, GRB 050820 shows a surprisingly good match to these characteristics. Although other processes could explain the N V gas associated with this GRB (e.g. diffuse gas in the galactic halo), one may associate this N V detection with shocked gas. Conversely, the remainder of N V detections have small velocity offsets from the ISM and do not exhibit broad line-profiles characteristic of $T \approx 10^5 \text{ K}$ gas. For the majority of the GRB sample, therefore, we must consider an alternative process. Furthermore, the absence of N V detections at $\delta v \ll 0 \text{ km s}^{-1}$ in these sightlines constrains the nature of stellar winds and the ISM. The data suggest that the stellar wind has a termination radius less than 10 pc such that the afterglow has photoionized this material. We will explore this latter idea at greater length in the next section.

3.4. Photoionization by the Afterglow

In the previous sections we argued that the halo and neutral ISM of the host galaxy as well as material shock-heated by the progenitor's stellar wind are unlikely to yield N^{+4} gas with characteristics resembling the majority of our GRB N V sample. Motivated by the narrow N V line-profiles, we turn to a model where the N^{+4} gas arises from photoionization. This cannot include ionization by an OB association because these stars emit far too few photons at $h\nu > 77 \text{ eV}$ to produce a meaningful column density of N^{+4} . Even a $40 M_{\odot}$ star emits too few photons during its lifetime to produce a significant N^{+4} column density. The progenitor stars of GRBs, however, may be very massive stars that undergo a Wolf-Rayet phase with effective temperatures exceeding 100,000 K (Hirschi et al. 2005; Hammer et al. 2006)¹⁰. These could produce measurable column densities of N^{+4} , but only at distances $r \ll 1 \text{ pc}$ from the WR star. We now demonstrate that this gas is photoionized by the GRB afterglow.

Owing to synchrotron processes, GRB afterglows have a roughly power-law spectrum with emission extending from the optical to X-ray frequencies. The afterglow, therefore, will initiate an ionization front giving highly ionized material at small radii ($r < 1 \text{ pc}$) and progressively less ionized gas at larger radii as the photon flux decreases by r^{-2} . The photon flux is sufficiently high that the r^{-2} dependence dominates over any attenuation (shielding) by the surrounding medium. One can estimate the distance where a specific ion (e.g. N^{+4}) will reach a maximum ionization fraction by comparing the photon flux f_{γ} which ionizes the next lower ionization state (i.e. N^{+3}) against the photoionization cross-section of that ion (i.e. $\sigma(\text{N}^{+3})$). For $f_{\gamma}\sigma \ll 1$, there will be a negligible ionization fraction. For $f_{\gamma}\sigma \gg 1$, it is likely that the ion will be fully ionized to a higher state. The peak in the ionization fraction is therefore likely to occur where $f_{\gamma}\sigma \sim 1$.

We can estimate this distance by adopting the afterglow of GRB 050730 which we parameterize as

$$L_{\nu} = 7.4 \times 10^{30} \left(\frac{h\nu}{80 \text{ eV}} \right)^{-1.8} \left(\frac{t_{\text{obs}}}{100 \text{ s}} \right)^{-0.3} \text{ erg s}^{-1} \text{ Hz}^{-1}. \quad (8)$$

¹⁰ Note that although rapidly rotating models suggest a higher flux of $h\nu \approx 100 \text{ eV}$ photons (Meynet, priv. communication), this will not change our conclusion.

Here, the frequency ν corresponds to the rest-frame and t_{obs} is time in the observer frame. We integrate from $t_{obs} = +10$ s (i.e. we ignore effects associated with the prompt phase) to $t_{obs} = +1000$ s which is a time typical for the onset of high-resolution spectroscopic observations. We calculate $\phi_\gamma = 3 \times 10^{58}$ photons emitted with energies in the interval $77 \text{ eV} < h\nu < 95 \text{ eV}$ which bounds the ionization potentials of N^{+3} and N^{+4} . At 1pc, this implies a photon flux of $f_\gamma \equiv \phi_\gamma / (4\pi r^2) = 2.4 \times 10^{20} \text{ cm}^{-2}$ which exceeds the column density of N nuclei for $n_H < 10^5 \text{ cm}^{-3}$ assuming a solar abundance (i.e. shielding is likely negligible). Finally, one compares the photon flux with the cross-section of N^{+3} , $\sigma(\text{N}^{+3})$. Using the parameterization of Verner et al. (1996), $\sigma(\text{N}^{+3}) = 10^{-18} \text{ cm}^2$ at $h\nu = 80 \text{ eV}$. The distance where N^{+4} should reach a maximum value is roughly where the photon flux matches the cross-section, i.e.,

$$r_{peak} \approx \left(\frac{\phi_\gamma \sigma(\text{N}^{+3})}{4\pi} \right)^{1/2} \quad (9)$$

or $\approx 15 \text{ pc}$ for our example.

We note that the spectral slope assumed here is steeper than most other afterglows and therefore implies a lower integrated photon luminosity at 100 eV than may be typical (some afterglows emit in excess of 10^{61} photons in the 77 to 95 eV interval). Furthermore, we have ignored the prompt emission of N^{+4} ionizing photons. Adopting the spectral parameterization of the prompt X-ray emission observed for GRB 060614 as an example (Butler & Kocevski 2007), we estimate 10^{58} photons emitted during the prompt phase $t_{obs} \leq 100$ s. This low redshift burst has a smaller X-ray luminosity than typical and we estimate the prompt phase can contribute in excess of 10^{60} photons. If E_{peak} evolves like t_{obs}^{-2} , then to first order the prompt and afterglow phases will have comparable time-integrated photon fluxes at 100 eV.

To verify the distance estimate above and to explore a range of physical conditions, we have performed a series of time-dependent, photoionization calculations for the propagation of ionizing flux through a constant density medium (e.g. Perna & Lazzati 2002). Our calculation follows the photons through a series of constant density, optically thin layers allowing for absorption by H, He, C, N, and O. We ignore recombinations because the timescales exceed (by orders of magnitude) the duration of the observations. In the following, we have adopted the afterglow of GRB 050730 integrating from $t_{obs} = +10$ s to $+1000$ s. In this respect, the calculation yields the ionization state of the gas that photons emitted at $t_{obs} = +1000 \text{ s} + \delta t$ would ‘observe’ on their travel to Earth.

The curves in Figure 3 show the ionization fractions of N^{+3} , N^{+4} , He^+ , and H^0 as a function of distance from the GRB afterglow for $n_H = 10 \text{ cm}^{-3}$. We find that the majority of nitrogen gas at $r_{peak} \approx 10 \text{ pc}$ has been photoionized to N^{+4} , while nitrogen gas at smaller distances is in higher ionization states and nitrogen gas at greater distances are in lower ionization states. The total N^{+4} column density predicted from this calculation (assuming $n_H = 10 \text{ cm}^{-3}$) is

$$N(\text{N}^{+4}) = 10^{14} \text{ cm}^{-2} \left[\frac{(\text{N}/\text{H})}{10^{-6}} \right] \quad [n_H = 10 \text{ cm}^{-3}], \quad (10)$$

where we note that $(\text{N}/\text{H}) = 10^{-6}$ corresponds to 1/100 solar abundance. This calculation shows that even a modest density, sub-solar gas can produce an N^{+4} column density consistent with the observations. We have repeated the calculations for a range of n_H values and find the N^{+4} column density scales with n_H for small n_H values but has an approximately $n_H^{1/2}$ dependence for $n_H > 5 \text{ cm}^{-3}$. The calculations also indicate that the N^{+4} ionic fraction peaks at a slightly smaller radius (by a few pc) for larger n_H but roughly the same position for smaller n_H values. These results are sensitive, however, to assumptions on the ionization state of the gas prior to the afterglow. Here, we have assumed the gas is neutral at $t_{obs} = 10$ s at all radii $r > 1 \text{ pc}$. If one allows for a pre-existing H II region extending to greater than 30 pc (e.g. Whalen et al. 2008), this gives more N^{+4} gas at larger radii and a larger total N^{+4} column density due to reduced shielding by H I gas but the differences are modest ($< 30\%$). We have also explored afterglows with a range of luminosities. This is identical to studying a single system at various times t_{obs} because the only relevant quantity is the integrated photon flux prior to the time of observation. Not surprisingly, both r_{peak} and the integrated N^{+4} column densities increase with the afterglow luminosity (Figure 4).

The results presented in Figure 3 and described above reveal a generic prediction for GRB afterglows. Just as the $\approx 6 \text{ eV}$ far-UV photons excite Si^+ and Fe^+ ions out to 1 kpc distance, the $\approx 80 \text{ eV}$ photons from the afterglow photoionize nearly all nitrogen at $r \approx 10 \text{ pc}$ to N^{+4} . Furthermore, the strengths of the N V absorption should not be correlated with H I column density and will at best be loosely correlated with the low-ion column density. These predications are consistent with the current sample of observations. The photoionization scenario described here will also imply significant absorption by other high-ions, e.g. C IV, O VI transitions. Figure 1 shows that we observed strong C IV absorption at the velocity of N V in every case. We find, however, that the signal-to-noise and line-blending in the current spectra prohibit a meaningful search for the O VI doublet. In summary, we predict detectable N V absorption in all GRB afterglow spectra except those where the gas at $r \approx 10 \text{ pc}$ has very low nitrogen density $n_N \equiv n_H (\text{N}/\text{H})$ or has been collisionally ionized to higher states (i.e. $T > 10^6 \text{ K}$).

A high temperature ($T > 10^6 \text{ K}$; shocked wind) and low density gas is in fact predicted at $r \approx 10 \text{ pc}$ in the stellar winds of GRB progenitors (e.g. van Marle et al. 2005). If we are to explain narrow N V absorption with small velocity offset from the neutral gas, one must conclude that the stellar wind does not extend beyond $r \approx 10 \text{ pc}$. Referring to equation 6, this implies

$$\rho_0 \gtrsim 8 \times 10^{-20} \left(\frac{L_{\text{ms}}}{10^{36} \text{ erg s}^{-1}} \right) \left(\frac{t_{\text{ms}}}{5 \times 10^6 \text{ yr}} \right)^3 \text{ g cm}^{-3}. \quad (11)$$

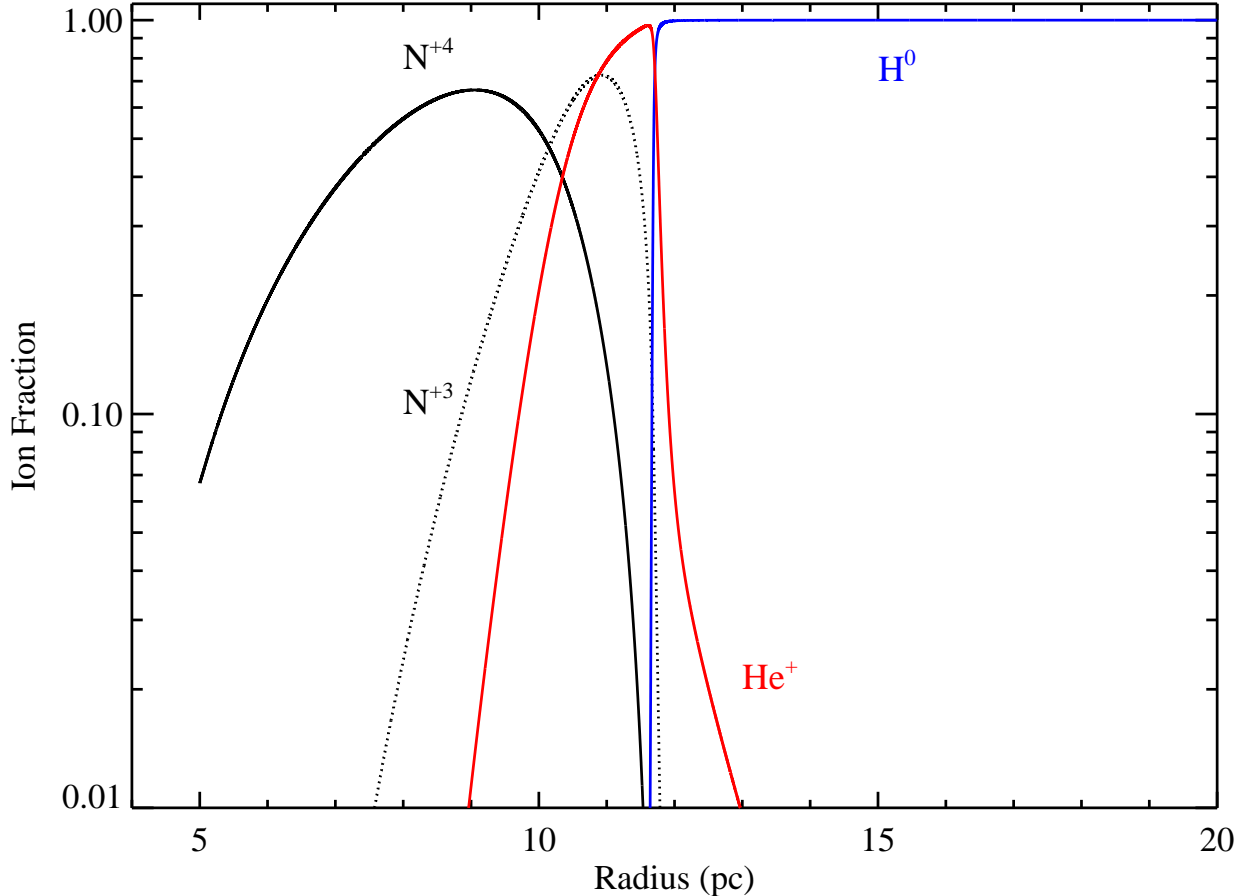


FIG. 3.— Ion fractions for a series of ions (i.e. X_i/X) as a function of distance from the GRB afterglow. The calculation assumes a constant density medium ($n_H = 10 \text{ cm}^{-3}$) and the total photon flux from an afterglow with L_ν = integrated from $t = +10\text{s}$ to $+1000\text{s}$ in the observer frame. Therefore, the calculations represent the ion fractions that a photon emitted at $t = +1000\text{s} + \delta t$ would ‘observe’ as it traveled through the medium.

This restriction is, however, only valid if the ISM is cold so that the circumstellar bubble expands supersonically with respect to the surrounding ISM. For a sufficiently high ISM temperature, the thermal pressure of the ISM will act as an extra confining force. An example of this is an H II region. In such an environment, the main sequence wind can never create a supersonically expanding shell. Pressure balance between the thermal pressure in the hot wind bubble and the thermal pressure of the ISM (with n_0 particle density)

$$P_0 = 10^{-10} \left(\frac{n_0}{1 \text{ cm}^{-3}} \right) \left(\frac{T}{10^6 \text{ K}} \right) \text{ dyne cm}^{-2}, \quad (12)$$

gives the radius of the wind termination shock

$$R_{\text{ms}} = 1.2 \left(\frac{\dot{M}_{\text{ms}}}{10^{-6} M_\odot \text{ yr}^{-1}} \right)^{1/2} \left(\frac{v_{\text{ms}}}{10^3 \text{ km s}^{-1}} \right)^{1/2} \left(\frac{P_0}{10^{-10} \text{ dyne cm}^{-2}} \right)^{-1/2} \text{ pc}. \quad (13)$$

Another scenario that would avoid the complications due to a steady stellar wind is a progenitor system that moves rapidly through the interstellar medium (e.g. Hammer et al. 2006; van Marle et al. 2006). A complimentary conclusion can be drawn from this analysis: GRB progenitor models that predict stellar winds extending beyond 10 pc must invoke a new process to explain the strong, narrow N V profiles with small offset observed for the majority of GRB sightlines.

These issues suggest an additional problem: Where is the gas related to afterglow photoionization in GRB 050820 for which one only observes relatively weak, broad N V absorption offset by $\delta v \approx -100 \text{ km s}^{-1}$ from the low-ion gas? In the previous section, we suggested that the N V gas for GRB 050820 may be explained by shock-heated gas associated with an expanding superbubble. Provided this bubble extends beyond 10 pc, the material photoionized by the afterglow will occur at $\delta v < 0 \text{ km s}^{-1}$. Furthermore, this gas is likely to have temperatures that ionize N beyond N^{+4} .

Adopting the afterglow photoionization model, we can use the observed N^{+4} column density to constrain n_N at $r \approx 10\text{pc}$ from the afterglow. Let us consider a few examples from the current sample under the assumption that the

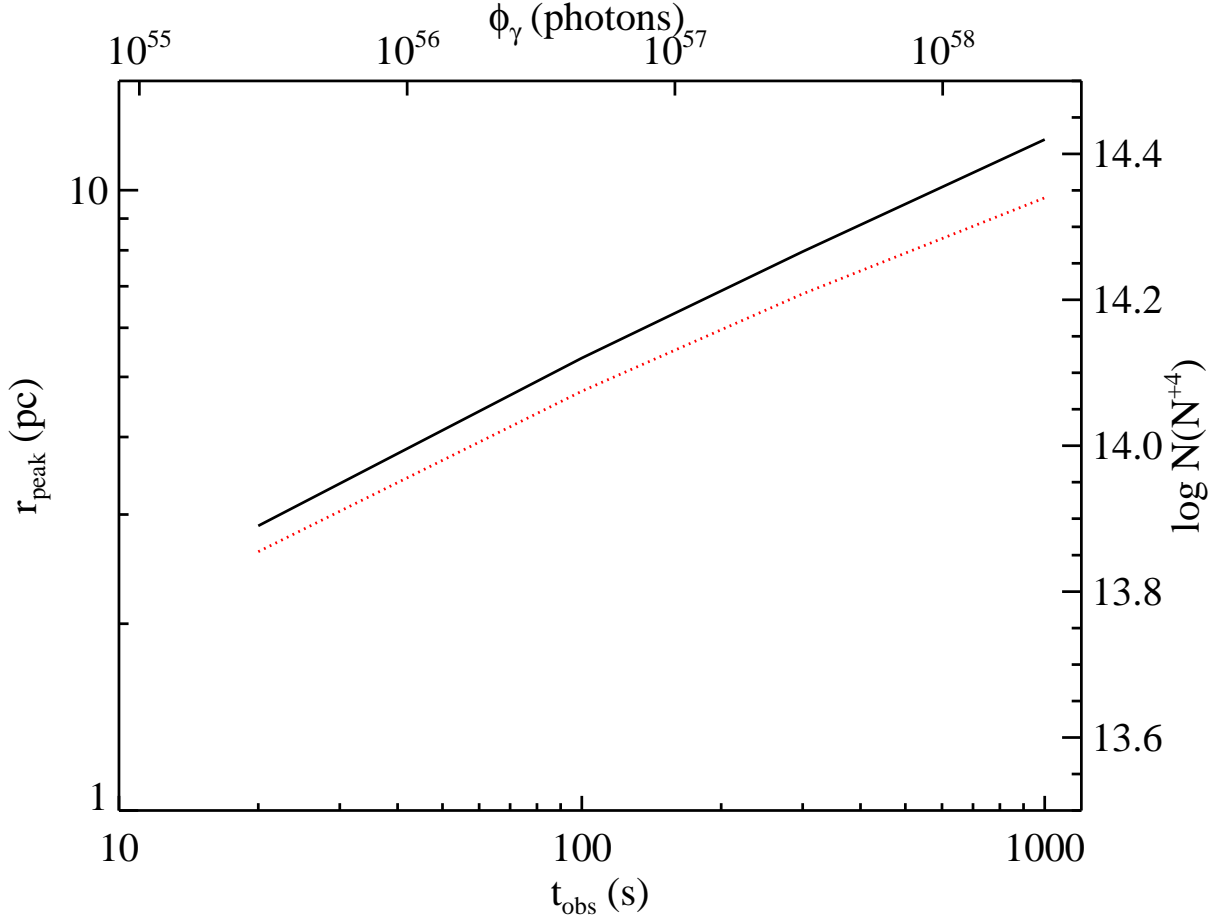


FIG. 4.— (solid black line): Evolution in the distance from the afterglow where the ionization fraction of N^{+4} peaks as a function of the time (x-axis) or number of ionizing photons (y-axis) emitted. (dotted red line): Evolution in the column density of N^{+4} as a function of the time (x-axis) or number of ionizing photons (y-axis) emitted. Both calculations assume the afterglow parameterization given by equation 8, $n_H = 1 \text{ cm}^{-3}$, and $[N/H] = -1$ dex.

afterglow ionization scenario is the only mechanism relevant to N^{+4} production. For those sightlines with $N(N^{+4}) \gtrsim 10^{14} \text{ cm}^{-2}$, we derive this constraint: $\log(n_H/\text{cm}^{-3}) + [N/H] \gtrsim -1$ dex. This is a relatively modest density and enrichment level; if GRB progenitors arise in star-forming regions, one may expect these conditions to be satisfied for nearly every GRB. The non-detection of N^{+4} gas toward GRB 060607, therefore, has a surprising implication. The upper limit of $N(N^{+4}) < 10^{12.6} \text{ cm}^{-2}$ gives $\log(n_H/\text{cm}^{-3}) + [N/H] < -2.7$ dex. This observation suggests both a metal-poor gas and a low-density medium surrounding the GRB. It is interesting to note that this GRB also shows the lowest H I column density of any GRB sightline to date (Chen et al. 2007b). This may indicate that some GRB events occur outside of both their star-forming regions and the ISM of the host galaxy.

If one allows that the metallicity of the neutral ISM (inferred from low-ion transitions) is applicable for the gas near the GRB, then one can constrain the n_H density alone. In a few cases (050730, 050820, 050922C), one observes N I transitions and can constrain N/H directly (Prochaska et al. 2007b). For example, the afterglow spectrum of GRB 050922C shows $[N/H] < -4$ and $N(N^{+4}) > 10^{14.2} \text{ cm}^{-2}$. This implies $n_H > 10^3 \text{ cm}^{-3}$ unless one assumes the gas is enriched in N local to the GRB (Dessauges-Zavadsky et al. 2008). We note that this density is comparable to the value needed to confine a stellar wind to $r < 10 \text{ pc}$ (see above). A summary of the constraints on the physical conditions for our dataset is given in Table 3.

Ultimately, the most valuable constraints may come from a time-series of spectroscopy (e.g. Vreeswijk et al. 2007) to investigate variability in the kinematics. Figure 4 indicates that r_{peak} increases by factors of a few during the first 1000s of the afterglow. Therefore, one would be sensitive to the kinematics of the gas at a range of radii allowing constraints on the differential motions at these distances. We have searched for temporal variations in the strength and velocity of the N V gas in the Keck/HIRES spectrum of GRB 050820 (two exposures of 900s starting at $t_{\text{obs}} \approx 3300\text{s}$) and the Magellan/MIKE spectrum of GRB 050730 (three 1800s exposures starting at $t_{\text{obs}} \approx 4\text{hr}$) (Prochaska et al. 2007a). The N V equivalent widths and line centroids are not observed to vary with statistical significance. We set upper limits of $\Delta W < 25 \text{ mÅ}$ and $\Delta v = 10 \text{ km s}^{-1}$ based on this modest S/N spectra.

TABLE 3
VOLUME DENSITY ESTIMATES

GRB	[N/H] ^a	log(n_H / cm ⁻³) ^b
GRB021004	-3.0*	2.3
GRB030323	-1.9*	< 0.9
GRB050730	-3.2	1.9
GRB050820	> -1.3	< -0.5
GRB050922C	< -4.1	> 3.0
GRB060206	-1.9*	0.3
GRB060607	-2.0*	< -0.7

^aNitrogen metallicity inferred from the ratio of N⁰ and H⁰ column densities (Prochaska et al. 2007b). This gas is located at a distance of 100pc to a few kpc from the GRB afterglow. Systems marked with a * do not have N I observations and we have set [N/H]=[M/H]-1.

^bScaled from our photoionization models assuming the afterglow (GRB050730) used throughout the paper.

4. CONCLUDING REMARKS

We have performed a survey of N V absorption along seven GRB sightlines and reported six positive detections within 100km s⁻¹ of the neutral gas associated with the host galaxy. Aside from the GRB 050820 sightline (where the N V absorption is broad, weak and offset by $\delta v \approx -100$ km s⁻¹), the N⁺⁴ gas has large column density and kinematically ‘cold’ line-profiles. The latter characteristic refers to a low velocity dispersion and a small offset $|\delta v| < 20$ km s⁻¹ from the neutral gas. The N V profiles are also coincident in velocity with fine-structure absorption which suggests the gas is located within ≈ 1 kpc of the GRB afterglow.

We have explored several scenarios that could produce N V absorption along GRB sightlines. Models related to the halo of the host galaxy or material shock-heated by the progenitor’s stellar wind are disfavored by the observations. In contrast, a scenario where the N⁺⁴ gas is material photoionized by the GRB afterglow naturally reproduces the observations provided the gas at $r \approx 10$ pc is cold ($T \approx 10^4$ K), and has a modest density ($n \approx 1$ cm⁻³), a non-negligible metallicity ([N/H] > -2), and a similar velocity as the ISM at $r \gtrsim 100$ pc.

The afterglow photoionization model places several important constraints on the progenitor and its environment. In particular, this scenario requires that the stellar wind of the progenitor terminates at less than $r \approx 10$ pc. This suggests the GRB progenitor has a weak, main-sequence stellar wind owing to a low mass-loss rate, a low wind speed, and/or a short lifetime. These characteristics may be a natural consequence of the progenitors that favor the GRB phenomenon, e.g. higher mass, lower metallicity stars. The wind can also be confined by introducing a dense ($n \gtrsim 10^3$ cm⁻³) external medium. Perhaps GRBs are preferentially embedded within the dense regions of molecular clouds as opposed to a violent, starburst region. On the other hand, we note that the N V absorption detected along the GRB 050820 sightline has characteristics consistent with shock-heated gas provided a shock with $v \approx 100$ km s⁻¹. In this case, we may be seeing the signatures of a starburst galaxy.

Before concluding, we wish to comment on a few directions for future research. One aspect to explore is how the soft X-ray absorption observed in the afterglow spectroscopy compares with the N⁺⁴ observations. To zeroth order, both measurements are sensitive to the column density of metals near the GRB progenitor, although likely at somewhat different radii. A comprehensive model of these observations may constrain the density profile of gas close to the GRB. Another implication of our research is that one predicts recombinations of the N⁺⁴ gas (and other high-ions, e.g. O⁺⁵) once the afterglow fades. For low z GRB, it may be possible to observe this line emission with a sensitive ultraviolet telescope (Perna et al. 2000). Finally, one predicts that other high ionization states will be produced by the afterglow (e.g. O⁺⁵, S⁺⁵) that could be studied in a similar fashion to constrain the relative abundances of gas near the progenitor star.

We acknowledge helpful discussions with D. Kasen and A.-J. van Marle. We thank D. Whalen and A. Heger for their calculations of the photon flux from massive stars. We thank S. Savaglio for providing her reduction of the VLT/UVES cb58 data for analysis. J. X. P. is partially supported by NASA/Swift grants NNG06GJ07G and NNX07AE94G and an NSF CAREER grant (AST-0548180). Based on observations made with ESO Telescopes at the Paranal Observatories and accessed from the ESO data archive.

REFERENCES

- Bowen, D. V., Jenkins, E. B., Tripp, T. M., Sembach, K. R., Savage, B. D., Moos, H. W., Oegerle, W. R., Friedman, S. D., Gry, C., Kruk, J. W., Murphy, E., Sankrit, R., Shull, J. M., Sonneborn, G., & York, D. G. 2007, ArXiv e-prints, 711
- Butler, N. R., & Kocevski, D. 2007, ApJ, 663, 407
- Campana, S., Lazzati, D., Ripamonti, E., Perna, R., Covino, S., Tagliaferri, G., Moretti, A., Romano, P., Cusumano, G., & Chincarini, G. 2007, ApJ, 654, L17

- Chen, H.-W., Prochaska, J. X., & Bloom, J. S. 2007a, *ApJ*, 668, 384
- Chen, H.-W., Prochaska, J. X., Bloom, J. S., & Thompson, I. B. 2005, *ApJ*, 634, L25
- Chen, H.-W., Prochaska, J. X., & Gnedin, N. Y. 2007b, *ApJ*, 667, L125
- Chen, H.-W., Prochaska, J. X., Ramirez-Ruiz, E., Bloom, J. S., Dessauges-Zavadsky, M., & Foley, R. J. 2007c, *ApJ*, 663, 420
- Dessauges-Zavadsky, M., Chen, H.-W., Prochaska, J. X., Bloom, J. S., & Barth, A. J. 2006, *ApJ*, 648, L89
- Dessauges-Zavadsky, M., Prochaska, J. X., & Chen, H.-W. 2008, In prep
- D'Odorico, V., Cristiani, S., Romano, D., Granato, G. L., & Danese, L. 2004, *MNRAS*, 351, 976
- Dupree, A. K., & Raymond, J. C. 1983, *ApJ*, 275, L71
- Eldridge, J. J., Genet, F., Daigne, F., & Mochkovitch, R. 2006, *MNRAS*, 367, 186
- Fiore, F., D'Elia, V., Lazzati, D., Perna, R., Sbordone, L., Stratta, G., Meurs, E. J. A., Ward, P., Antonelli, L. A., Chincarini, G., Covino, S., Di Paola, A., Fontana, A., Ghisellini, G., Israel, G., Frontera, F., Marconi, G., Stella, L., Vietri, M., & Zerbi, F. 2005, *ApJ*, 624, 853
- Fox, A. J., Petitjean, P., Ledoux, C., & Srianand, R. 2007, *A&A*, 465, 171
- Galama, T. J., & Wijers, R. A. M. J. 2001, *ApJ*, 549, L209
- García-Segura, G., Langer, N., & Mac Low, M.-M. 1996, *A&A*, 316, 133
- Hammer, F., Flores, H., Schaerer, D., Dessauges-Zavadsky, M., Le Floc'h, E., & Puech, M. 2006, *A&A*, 454, 103
- Heckman, T. M., & Leitherer, C. 1997, *AJ*, 114, 69
- Herrero, A., Kudritzki, R. P., Vilchez, J. M., Kunze, D., Butler, K., & Haser, S. 1992, *A&A*, 261, 209
- Hirschi, R., Meynet, G., & Maeder, A. 2005, *A&A*, 443, 581
- Humphreys, R. M. 1991, in *IAU Symposium*, Vol. 143, *Wolf-Rayet Stars and Interrelations with Other Massive Stars in Galaxies*, ed. K. A. van der Hucht & B. Hidayat, 485–+
- Indebetouw, R., & Shull, J. M. 2004a, *ApJ*, 605, 205
- . 2004b, *ApJ*, 607, 309
- Jakobsson, P., Fynbo, J. P. U., Ledoux, C., Vreeswijk, P., Kann, D. A., Hjorth, J., Priddey, R. S., Tanvir, N. R., Reichart, D., Gorosabel, J., Klose, S., Watson, D., Sollerman, J., Fruchter, A. S., de Ugarte Postigo, A., Wiersema, K., Björnsson, G., Chapman, R., Thöne, C. C., Pedersen, K., & Jensen, B. L. 2006, *A&A*, 460, L13
- Lazzati, D., & Perna, R. 2002, *MNRAS*, 330, 383
- Ledoux, C., Vreeswijk, P., Smette, A., Jaunsen, A., & Kaufer, A. 2006, *GRB Coordinates Network*, 5237, 1
- Perna, R., & Lazzati, D. 2002, *ApJ*, 580, 261
- Perna, R., Raymond, J., & Loeb, A. 2000, *ApJ*, 533, 658
- Pettini, M., Rix, S. A., Steidel, C. C., Adelberger, K. L., Hunt, M. P., & Shapley, A. E. 2002, *ApJ*, 569, 742
- Piranomonte, S., Ward, P., Fiore, F., & Others, A. 2007, *A&A*
- Prochaska, J. X., Chen, H.-W., & Bloom, J. S. 2006, *ApJ*, 648, 95
- Prochaska, J. X., Chen, H.-W., Bloom, J. S., Dessauges-Zavadsky, M., O'Meara, J. M., Foley, R. J., Bernstein, R., Burles, S., Dupree, A. K., Falco, E., & Thompson, I. B. 2007a, *ApJS*, 168, 231
- Prochaska, J. X., Chen, H.-W., Dessauges-Zavadsky, M., & Bloom, J. S. 2007b, *ApJ*, 666, 267
- Prochaska, J. X., Chen, H.-W., Wolfe, A. M., Dessauges-Zavadsky, M., & Bloom, J. S. 2008, *ApJ*, 672, 59
- Prochaska, J. X., Wolfe, A. M., Howk, J. C., Gawiser, E., Burles, S. M., & Cooke, J. 2007c, *ArXiv Astrophysics e-prints*
- Ramirez-Ruiz, E., García-Segura, G., Salmonson, J. D., & Pérez-Rendón, B. 2005, *ApJ*, 631, 435
- Ramirez-Ruiz, E., Trentham, N., & Blain, A. W. 2002, *MNRAS*, 329, 465
- Savage, B. D., & Sembach, K. R. 1991, *ApJ*, 379, 245
- Savage, B. D., Sembach, K. R., & Lu, L. 1995, *ApJ*, 449, 145
- . 1997, *AJ*, 113, 2158
- Savaglio, S., Fall, S. M., & Fiore, F. 2003, *ApJ*, 585, 638
- Savaglio, S., Panagia, N., & Padovani, P. 2002, *ApJ*, 567, 702
- Sembach, K. R., Wakker, B. P., Savage, B. D., Richter, P., Meade, M., Shull, J. M., Jenkins, E. B., Sonneborn, G., & Moos, H. W. 2003, *ApJS*, 146, 165
- Shapley, A. E., Steidel, C. C., Pettini, M., & Adelberger, K. L. 2003, *ApJ*, 588, 65
- Shull, J. M., & McKee, C. F. 1979, *ApJ*, 227, 131
- Slavin, J. D., & Cox, D. P. 1992, *ApJ*, 392, 131
- Slavin, J. D., Shull, J. M., & Begelman, M. C. 1993, *ApJ*, 407, 83
- Tenorio-Tagle, G., Bodenheimer, P., & Rozyczka, M. 1987, *A&A*, 182, 120
- Thöne, C. C., Wiersema, K., Ledoux, C., Starling, R. L. C., Fynbo, J. P. U., Curran, P. A., Gorosabel, J., van der Horst, A. J., Kewley, L. J., Levan, A. J., Llorente, A., Rol, E., Tanvir, N. R., de Ugarte Postigo, A., Vreeswijk, P. M., & Wijers, R. A. M. J. 2007, *ArXiv e-prints*, 708
- Thöne, C. C., Greiner, J., Savaglio, S., & Jehin, E. 2007, *ApJ*, 671, 628
- Tumlinson, J., Prochaska, J. X., Chen, H.-W., Dessauges-Zavadsky, M., & Bloom, J. S. 2007, *ApJ*, 668, 667
- van Marle, A. J., Langer, N., Achterberg, A., & García-Segura, G. 2006, *A&A*, 460, 105
- van Marle, A. J., Langer, N., & García-Segura, G. 2005, *A&A*, 444, 837
- van Marle, A. J., Langer, N., Yoon, S.-C., & García-Segura, G. 2007, *ArXiv e-prints*, 711
- Verner, D. A., Ferland, G. J., Korista, K. T., & Yakovlev, D. G. 1996, *ApJ*, 465, 487
- Vreeswijk, P. M., Ellison, S. L., Ledoux, C., Wijers, R. A. M. J., Fynbo, J. P. U., Møller, P., Henden, A., Hjorth, J., Masi, G., Rol, E., Jensen, B. L., Tanvir, N., Levan, A., Castro Cerón, J. M., Gorosabel, J., Castro-Tirado, A. J., Fruchter, A. S., Kouveliotou, C., Burud, I., Rhoads, J., Masetti, N., Palazzi, E., Pian, E., Pedersen, H., Kaper, L., Gilmore, A., Kilmartin, P., Buckle, J. V., Seigar, M. S., Hartmann, D. H., Lindsay, K., & van den Heuvel, E. P. J. 2004, *A&A*, 419, 927
- Vreeswijk, P. M., Ledoux, C., Smette, A., Ellison, S. L., Jaunsen, A. O., Andersen, M. I., Fruchter, A. S., Fynbo, J. P. U., Hjorth, J., Kaufer, A., Møller, P., Petitjean, P., Savaglio, S., & Wijers, R. A. M. J. 2007, *A&A*, 468, 83
- Watson, D., Hjorth, J., Fynbo, J. P. U., Jakobsson, P., Foley, S., Sollerman, J., & Wijers, R. A. M. J. 2007, *ApJ*, 660, L101
- Weaver, R., McCray, R., Castor, J., Shapiro, P., & Moore, R. 1977, *ApJ*, 218, 377
- Welsh, B. Y., & Lallement, R. 2005, *A&A*, 436, 615
- Whalen, D., Prochaska, J. X., Heger, A., & Tumlinson, J. 2008, *ArXiv e-prints*, 802
- Willis, A. J. 1991, in *IAU Symposium*, Vol. 143, *Wolf-Rayet Stars and Interrelations with Other Massive Stars in Galaxies*, ed. K. A. van der Hucht & B. Hidayat, 265–+
- Wolfe, A. M., Gawiser, E., & Prochaska, J. X. 2005, *ARA&A*, 43, 861
- Woosley, S. E., & Bloom, J. S. 2006, *ARA&A*, 44, 507
- Zwaan, M. A., & Prochaska, J. X. 2006, *ApJ*, 643, 675